[J. Krüger, J. Koppmann, P. Nau, A. Brockhinke, M. Schenk, N. Hansen, U. Werner, K. Kohse-Höinghaus, From precursors to pollutants:
Some advances in combustion chemistry diagnostics, Eurasian Chemico-Technological Journal 16 (2014) 91–105.]

The original publication can be accessed via ISSN: 1562-3920

From precursors to pollutants:

Some advances in combustion chemistry diagnostics

Julia Krüger[1], Julia Koppmann[1], Patrick Nau[1,2], Andreas Brockhinke[1], Marina Schenk[1], Nils Hansen[3], Udo Werner[4], and Katharina Kohse-Höinghaus[1]*

[1]Department of Chemistry, Bielefeld University, Universitätsstraße 25, D-33615 Bielefeld, Germany

[2]now at Institute of Combustion Technology, German Aerospace Center (DLR), Pfaffenwaldring 38-40, D-70569 Stuttgart, Germany

[3]Combustion Research Facility, Sandia National Laboratories, Livermore, CA 94551, USA

[4]Department of Physics, Bielefeld University, Universitätsstraße 25, D-33615 Bielefeld, Germany

*Corresponding author; Email: kkh@uni-bielefeld.de, Phone: +49 521 106-2052

Full-length article

Abstract

The present assessment and prediction of potential pollutant emissions from combustion systems often rely on dedicated combustion models. Their validation depends on the critical examination of the relevant chemical reaction pathways. To this end, a number of combustion diagnostic techniques are available which can probe important chemical constituents *in situ*, thus providing direct information on the progress of the combustion reactions. Here, some recent experimental advances for the investigation of a suite of targets from molecular intermediates and soot precursors to nascent particles will be presented. Examples include the application of quantum cascade laser absorption spectroscopy (QCLAS), molecular-beam mass spectrometry (MBMS) with different ionization schemes, photoelectron–photoion coincidence (PEPICO) spectroscopy, helium ion microscopy (HIM), and polarization-modulated infrared reflection–absorption spectroscopy (PM-IRRAS).

1. Introduction

Pollutants formed by the combustion of conventional and alternative fuels are of major influence on human health and the environment. With stricter regulations and growing public awareness regarding air quality, especially in urban areas in many countries of the world, pollutant prevention or abatement is an urgent target in combustion research. Recent reports of the Intergovernmental Panel of Climate Change [1] and the World Health Organization [2] underline the urgency of actions regarding the reduction of particulate matter emissions from combustion sources. Investigations of pollution in large, densely inhabited urban areas have also identified photochemically active substances such as carbonyl compounds, probably enhanced by use of first-generation biofuels, as causes of respiratory and other health problems [3,4]. While significant reductions in emissions have already resulted from stricter regulations on the one hand, as documented e.g. in the progress of European emission standards [5], the increase in industrialization and transportation on the other is cause for eminent concern: The average number of cars per 1000 persons in all Asia, for example, has grown to about 65 in 2010, while it stagnated near 800 in the USA, with a value of 65 in the USA reached at the end of the First (!) World War [6]. Rapid development in China is reported to contribute to an exponentially increasing inventory of non-methane volatile organic compounds (NMVOCs), involved in photo-oxidative processes deteriorating air quality, such as alkenes, alkynes, aromatics, and carbonyl species [7]. As most prognoses predict that the global contribution of fossil resources to the energy conversion will only very gradually – over decades – decrease from the present high value of >85% [8,9], huge efforts are necessary to make combustion cleaner.

Such strategies for cleaner combustion processes in transportation include low-temperature combustion and the use of biofuels. Even for advanced low-temperature diesel engines equipped with oxidation catalysts Li and Ogawa [10] have recently reported unregulated harmful emissions such as carbonyls, aromatics, and 1,3-butadiene to increase with high ex-

haust gas recirculation. Also, He et al. [11,12] have shown that use of *n*-butanol, a promising biofuel, or its addition to gasoline in homogeneous charge compression ignition (HCCI) engines may significantly increase acetaldehyde and formaldehyde emissions. A closer inspection of the chemical composition of unregulated emissions and their formation reactions is thus needed, with the challenge, however, that these depend highly on the combustion process, its physico-chemical conditions, and the specific fuel or fuel blend.

Combustion emissions are typically predicted using numerical simulations with detailed combustion models. Computational combustion [13], with simulations relying on kinetic information for complex mechanisms such as soot formation [14,15], has become an important field in combustion research. Detailed models to describe the combustion mechanism can be established if all physical and chemical information on the process is known, including its initial or boundary conditions, the course of the combustion reactions, and the interactions of the system with the environment. Ideally, all kinetic, transport, and thermochemical data are then included for the complete set of combustion reactions [16]. For realistic fuels, more than 10,000 elementary steps may contribute to the overall combustion reaction [17].

Although such reaction sets may be consistently and systematically generated, their reliability depends on their critical examination and validation against a broad range of conditions encompassing the relevant regimes of pressure, temperature, and mixture composition. To this end, the field of combustion diagnostics, established more than 30 years ago (compare, for example, the biannual Gordon Research Conference series on Laser Diagnostics in Combustion, started in 1981), has contributed numerous techniques that are suitable for a direct inspection of the combustion process [18-22]. Regarding intermediate species concentrations and finer details of the combustion chemistry, including the detection of reactive intermediates, laser methods have been established and complemented with *in situ* molecular-beam mass spectrometry (MBMS), which permits sampling and chemical analysis e.g. from flames, shock tubes, and chemical reactors [23-28]. Using photoionization (PI) MBMS techniques,

separation of the different isomeric structures is possible [29,30], with one first example being the distinction of acetaldehyde and ethenol in flames [29], followed by many other applications. PI-MBMS has allowed, for example, to distinguish between different carbonyl species formed from combustion of the four isomers of butanol [31] as prototypical oxygenated (bio-)fuels, or between the different soot precursor structures formed in the combustion of cyclopentene [32] as a cycloalkene component of conventional fuels.

It is beyond the scope of this article to characterize the multitude of experimental methods available today regarding their merits and potential shortcomings for combustion chemistry research. Rather, some recent examples shall be given, involving the work of our own group and of selected collaboration partners, to illustrate some advances in chemical combustion diagnostics. Such techniques may offer perspectives, on the one hand, to provide new insights into the formation reactions of regulated and unregulated pollutants as a function of fuel structure and combustion conditions, and on the other, may permit careful examination and further development of kinetic mechanisms for combustion.

2. Experimental methods and procedures

Details of the experiments have been reported in several earlier publications, and only some information is given here to assist with understanding the principles of the techniques and the selected examples presented in this contribution.

2.1 Burners and flames

Examples in this article are from different flame configurations. For the measurement of mole fraction profiles in laminar premixed low-pressure flames, a flat matrix burner made from sintered bronze (McKenna type) with a diameter of 66 mm was used. Dimethyl ether (DME)-oxygen flames diluted with argon were stabilized at 33 mbar for equivalence ratios ϕ=0.93 and 1.40 [33,34] with gas flows (in slm, *i.e.* standard liters per minute, at 300 K) of 0.85

(1.13) DME and 2.72 (2.42) O_2; the rich condition is given in parentheses. Both flames were diluted with 1.21 slm Ar, and cold gas velocities at 300 K were calculated to be between 0.77 and 0.78. Conditions were chosen to match approximately those of Wang et al. [35]. For the experiments using quantum cascade laser absorption spectroscopy (QCLAS), a variant of the burner was built up which featured an additional, separate concentric bronze matrix of 20 mm width for an inert co-flow to prevent mixing of combustion products into the beam paths. For all investigations of low-pressure premixed flames in this work, burners of near-identical configuration in different burner chambers were used that were adapted to the respective geometries for the laser and MBMS measurements in Bielefeld and the PEPICO experiment performed at the SOLEIL synchrotron in France. In the latter, a ϕ=1.6 DME-O_2 flame diluted with 25% argon at 33 mbar was studied, again closely adapted to one of the conditions reported by Wang et al. [35].

Non-premixed flames were investigated in an opposed-flow configuration at atmospheric pressure, with *n*-butane as the fuel, and procedures as detailed in [36]. The mole fraction compositions of the opposing gas streams and corresponding mass flow rates were 0.06 *n*-C_4H_{10} / 0.94 Ar at a mass flow rate of 3.2×10^{-2} g cm^2 s^{-1}on the fuel side and 0.38 O_2 / 0.62 Ar with a mass flow rate of 2.9×10^{-2}g cm^2 s^{-1}on the oxidizer side.

Soot was sampled from fuel-rich ethene flames stabilized at atmospheric pressure on a porous plug burner (50 mm diameter) with a configuration from Abid et al. [37] that was reproduced for our own work; details on flames and the setup have been discussed elsewhere [38,39]. Specifically, soot formed at the condition of their flame C3 [37] was studied here with a composition of 16.3% C_2H_4, 23.7% O_2, and 60% Ar, at a cold gas velocity of 8 cm/s at 298 K and a temperature of 1736±50 K.

2.2 Quantum cascade laser absorption spectroscopy (QCLAS)

For the quantum cascade laser absorption measurements, a low-pressure burner configuration described in [33,34] was used featuring three QCL units (Cascade Technologies) at 4.5 μm, 5.9 μm, and 7.8 μm. The lasers were individually controlled by a controller unit and operated at pulse lengths of 500 ns and a repetition rate of 20 kHz. The laser beams were combined by several sets of mirrors and focused into the burner chamber by a CaF_2 lens. Beam profiles were shaped by suitable pinholes. After transmission through the burner chamber, the beams were focused with an off-axis parabolic mirror onto an IR detector (Vigo Systems PVI-2TE). The signals were then digitized and processed. Care was taken to reduce reflections and stray light, using an anodized black aluminum chamber and windows mounted in Brewster's angle to permit complete transmission of radiation with polarization parallel to the plane of incidence. Window surfaces were deliberately placed at an angle to avoid etaloning effects. Inside the cylindrical window supports, the laser beams were guided through N_2-purged tubes of a few mm diameter into close proximity of the flame so that accumulation of combustion gases in these regions was minimized. Wavelength calibration was performed with the aid of an N_2O calibration gas cell and a Ge-etalon. Edge effects of the flame were removed by tomographic reconstruction using procedures from the literature [40,41].

2.3 Electron ionization (EI) mass spectrometry (MS) and gas chromatography (GC)

Molecular-beam mass spectrometry (MBMS) to analyze low-pressure flame chemistry has been described in detail before [23,42,43]. In most examples reported here, electron ionization (EI) was used to ionize flame-sampled species. Reflectron time-of-flight mass spectrometer setups with two-stage Wiley-McLaren configurations of the ion source were used to analyze the species composition in low-pressure premixed flat flames (with a mass resolution of up to 4000), and in atmospheric-pressure non-premixed flames (with mass resolution of ~2500). From the premixed flames, gas samples were extracted by a quartz nozzle (200 μm orifice diameter) and expanded into an intermediate chamber ($<10^{-3}$ mbar). The resulting molecular

beam passed through a skimmer into the ionization volume (at or below ~10^{-6}) mbar. Species were ionized and the resulting ions were detected with a multichannel plate. Mass spectra for all species were recorded according to the mass/charge (*m/z)* ratio of the ions, with argon serving as reference. Quantitative species profiles including radicals were obtained using procedures detailed in [42,43], typically as a function of height above the burner; the elemental composition of C/H/O species detected in the flames was determined by their exact mass.

For the study of the non-premixed flames, the flat-flame burner was replaced with the home-built opposed-flow burner system [44] operating at ambient pressure. Here, the gases were sampled with a microprobe (with 20 μm orifice), in analogy to the setup described in [45]. Only stable species were accessible with this technique. The fuel-rich zone in this configuration offers more facile access to the detection of higher-molecular growth species than the premixed flames. In this case the mass spectrometer was coupled to a GC instrument (Trace GC, Thermo Fisher Scientific) to access additional isomer-specific information. A low-polarity column (Restek, Rxi-5Sil MS) was used to separate some intermediates, including polycyclic aromatic hydrocarbons (PAHs), following the procedure detailed in [36]. Identification relied on chromatograms from reference substances and the manufacturer's database.

2.4 Photoelectron–photoion coincidence (PEPICO) spectroscopy in flames

Expanding the capabilities of EI-MBMS and isomer-selective PI-MBMS using VUV radiation from synchrotrons [23,25,29,46], PEPICO spectroscopy is a technique new to combustion diagnostics for which it was demonstrated only very recently [47-49]. This approach combines features of photoionization mass spectrometry with photoelectron spectroscopy and detects the ion–electron coincidence upon each single ionization event, typically using time-of-flight mass spectrometry for ion detection and velocity map imaging for electron detection.

The work was performed at the SOLEIL synchrotron in St. Aubin, France. A transportable burner and intermediate chamber were adapted to the SAPHIRS endstation at the DESIRS beamline equipped with the double-imaging PEPICO spectrometer DELICIOUS III [50]. The molecular beam was crossed with the VUV beam and the generated ions and electrons were detected with the DELICIOUS III spectrometer, which couples a Wiley-McLaren TOF analyzer/3D momentum imager on the ion side (with a mass resolution of ~300) to a velocity map imager on the electron side. Ions and electrons from an ionization event were registered in coincidence, using the detection of the electron to trigger the ion signal registration. By scanning the photon energy, mass-selected threshold photoelectron spectra can be obtained with an ultimate energy resolution <1 meV, although here we used 3.5 meV, largely sufficient for the scientific purpose. Selected spectra at fixed photon energies were taken in an energy range of 9-12 eV and a resolution of 70 meV with the photon energy above the ionization energy of the target species to record photoelectron spectra for a given mass.

2.5 Soot diagnostics with helium ion microscopy (HIM) and polarization-modulated infrared reflection–absorption spectroscopy (PM-IRRAS)

Soot particles were thermophoretically collected by motor-controlled rapid insertion of a substrate (silicon wafer with natural oxide layer, area ~1 cm^2) into the flame zone [38,39]. The substrate was affixed on a sample holder that was mounted on a stepper motor; the exposure time to the flame was typically ~16 ms. The investigated ethene flame (C3) was chosen from a larger set of flames that had been characterized before by Abid et al. [37].

Freshly deposited soot samples were analyzed by HIM with a delay of typically 15 min. HIM uses a fine beam of helium ions to scan the surface under investigation, and the emitted secondary electrons are detected. A Carl Zeiss Orion Plus HIM instrument was operated at ~35 kV with a beam current between 0.3 and 1 pA and a beam dwell time per pixel between 10 and 30 µs. All HIM micrographs were recorded with a pixel size of 0.5 nm. Details have

been described in [38,39]. The particles imaged by HIM were further analyzed with regard to their geometric properties using ImageJ software [51] with the Fraclac plugin; as detailed in [39], the particle perimeter, its area, the diameter of a circle which fully encloses the particle, and the fractal dimension were determined.

For the PM-IRRAS measurements, soot was deposited on a gold-coated silicon wafer. In this case, soot sampling was performed with the sampling device integrated into the stagnation plate as in the configuration of Abid et al. [52], with a sampling orifice of 0.5 mm diameter. Analysis was carried out with a Bruker PM-IRRAS instrument (Vertex 70-PMA50), using averages over 722 scans and an aperture of 1.5 mm. Alternating irradiation of the sample with perpendicularly or parallel polarized IR radiation provided an intrinsic reference.

3. Results and discussion

The examples in this work have been chosen to present selected combustion diagnostic approaches that have been recently introduced and hold promise for flame investigations. From this perspective, a comprehensive discussion of the respective combustion systems and relevant chemical reaction mechanisms is not intended. Rather, the results are reported to illustrate advances that may be possible using these methods in combustion investigations.

3.1 Intermediate species detection in low-pressure DME flames using QCLAS and MBMS

Among alternative fuels, dimethyl ether, which can be produced from coal, natural gas, and biomass, receives high attention, especially as a diesel additive or diesel substitute [53]. Because the DME molecule has no carbon-carbon bond, soot precursors are not easily built up and PAH and soot emissions are low. Flames of conventional hydrocarbon and other oxygenated fuels show, however, that in DME flames, the air toxic formaldehyde can be formed in comparatively high concentrations [54]. Recent engine studies with DME have shown formaldehyde to be a prominent exhaust component [55]. The combustion chemistry of DME

has been studied in detail [35,56,57], with a recent focus on low-temperature reaction kinetics [58-61]. Reasons for this are the two-step ignition behavior and the interest in combustion strategies such as homogeneous charge compression ignition. Kinetic mechanisms for DME are available since more than a decade [62-64], with recent improvements addressing specifically the low-temperature behavior [65]. For practical applicability, such mechanisms are being tested under a wide range of combustion conditions, including high pressures and dilution with exhaust gas components such as CO_2 [66]. While many details in the reaction scheme can be thought of as well understood, the accurate prediction of intermediate species is still under debate. In the low-temperature regime, recent measurements of species including HO_2, H_2O_2, formic acid, methyl formate, and others [59,61,67,68] show room for model improvement; also, the influence of (reactive) CO_2 suggests that attention should be devoted to some intermediate species reactions [66].

Many experimental measurements of intermediate species concentrations rely on different variants of mass spectrometry, a technique that is necessarily intrusive because it uses sampling probes to extract the gas sample to be analyzed from the reactive environment. Disturbances by such probes are being critically analyzed [69,70] and systematically modeled [71]. Whenever possible, it is preferable to probe the reactive gases with non-invasive optical means. Absorption spectroscopy with quantum cascade lasers offers excellent potential for such analyses, because they can probe all relevant molecules in their strong fundamental vibrations, and QCLAS has recently been demonstrated as a well-suited technique to analyze combustion-related environments in shock tubes and flames [72-77].

In our own work, we have combined QCLAS with MBMS to study dimethyl ether combustion. Figure 1 shows the CO and CO_2 mole fractions as a function of height above the burner h in two flat premixed DME-O_2-Ar flames of different stoichiometry, obtained from measurements with the QCL near 4.5 µm after selecting suitable spectral lines in this range [78]. The temperature was also determined with QCLAS, using the intensity ratio of suitable

absorption lines [75,77] from measurements of two CO and multiple CO_2 lines in the region of 2231.39-2232.00 cm^{-1}. In addition, the feasibility of temperature measurements was also examined using H_2O lines accessible with the QCL at 7.8 μm and from H_2O and CH_2O lines in the regime covered by the 5.9 μm laser; the results were found to be in quite good agreement [34]. Both flames shown in Fig. 1 were selected from the set of five stoichiometries studied by Wang et al. with EI- and PI-MBMS [35]. For comparison, the EI-MBMS profiles from [35] are included in Fig. 1, as well as simulations with the model by Zhao et al. [64] using the Cantera software package [79]. For the simulations, the optically measured, *i.e.* unperturbed, temperature profiles were used as input data without application of any shifts. Uncertainties for the absolute concentrations are within ~10-15% for the two detection methods. Within these uncertainties, very good agreement is seen for both profile shapes and absolute values. The CO mole fraction attains maximum values of ~0.15-0.20 and exhibits a maximum in both cases, with a plateau of ~0.075 in the lean and ~0.18 in the rich flame, while CO_2 reaches constant values near 0.20 in the former and 0.15 in the latter. Overall good agreement is also found with the simulation. Thus, for these main components in the flames, non-invasive QCLAS and perturbative MBMS measurements mutually enhance the confidence in these quantitative results for critical model examination and validation.

It is crucial to evaluate the effects of probe interference for combustion intermediates in great detail, because reliable intermediate concentrations are a pertinent test for reaction pathways and kinetic mechanisms. Formaldehyde, CH_2O, was chosen as a prominent intermediate in DME flames to investigate such influences [76]. Figure 2 shows a spectrum for CH_2O detection using the QCL at 5.9 μm in the ϕ=1.40 DME flame. The upper half in Fig. 2 represents the measured spectrum, and the lower half (as a mirror image) reports simulations for the contributions by CH_2O and H_2O obtained with the HITRAN /HITEMP databases [80]. The simulations were carried out for a flame temperature of 1100 K for the position at h=0.7 mm, very early in the flame and well upstream of the temperature maximum (compare Fig. 1).

It is in these cooler flame regions that CH_2O, indicative of low-temperature combustion reactions [62-65], is abundant.

The CH_2O profiles for the two DME flames are given in Fig. 3; note that the height axis shows only the first 5 mm above the burner. Again, QCLAS results are compared with EI-MBMS measurements from [35] and simulations with the Zhao et al. mechanism [64]. Experimental uncertainties for CH_2O are ≤15% for QCLAS [76] and 30% for the MBMS measurements [35]. As seen from Fig. 3, absolute maximum values are in quite reasonable agreement for both flames within these uncertainties, with peak mole fractions of ~0.012 near h=0.5 mm in the lean flame and of 0.017 (MBMS) vs. 0.025 (QCLAS) near h=0.7 mm in the rich flame, at the location at which the spectrum in Fig. 2 was taken. Striking, however, is the difference in the measured profiles, which appear shifted by almost 2 mm downstream for the MBMS measurements. The original paper by Wang et al. [35] reports shifts of 0.9 mm that they have consistently applied between both their EI-MBMS and PI-MBMS experiments and their simulation to account for probe effects and relates them to be about 1.3 (4) times the orifice diameter of the sampling cone of 0.7 mm (0.25 mm) for EI-MBMS (PI-MBMS). While such shifts have regularly been used in the literature to account for differences between mass spectrometric measurement and flame model simulations, it has been demonstrated that multiple parameters of the sampling configuration must be considered and that such influences are not necessarily constant with flame conditions, position in the flame, and species probed [69-71].

Here, in the example in Fig. 3, a near worst-case situation is probed, with the sampling cone very close to the burner surface, inserted into a chemically delicate region where both low-temperature reactions and high-temperature chemistry can be active [60,61,64,65] and where local cooling may affect their interplay. Several influences may contribute to the strong probe effect seen here: local perturbation of the flow (with the flame "squeezed" between burner and probe), local cooling by the sampling probe itself, attachment of the flame to the probe, and local cooling by the flange that holds the sampling probe, which is in this position

much closer to the flame than at the temperature maximum at 4-5 mm or in the burnt gases. Formaldehyde will also be much more sensitive to a number of reactions crucially influencing the early chemistry than carbon dioxide as a final product. Thus, the rather good agreement noted in Fig. 1 and the magnitude of the shift in Fig. 3 are not contradictory.

Additionally, simulations with the Zhao et al. model [64] are included in Fig. 3, using an unperturbed, optically measured temperature profile. A "perturbed" temperature profile as described in [70], determined from the gas stream passing through the sampling cone orifice in the EI-MBMS measurements, was not available in [35]. Application of such a "perturbed" profile to model the invasive MBMS measurements would be preferable, and an improved match between MBMS experiment and model (as e.g. in [42]) would be expected. It should be stressed, however, that with the wider availability of quantum cascade lasers, non-invasive QCLAS can be applied routinely for a larger number of species, including many stable intermediates. QCL diagnostics has also been demonstrated very recently to be able to detect very important fragile compounds such as hydrogen peroxide [74]. Thus, unavoidable systematic errors such as probe effects from using invasive techniques can be examined and corrected, and complementary QCLAS and MBMS experiments can improve the reliability of combustion chemistry studies.

3.2 Formaldehyde detection in a low-pressure DME flame using PEPICO spectroscopy

While EI-MBMS as a typical laboratory configuration permits a rapid overview of the chemical composition of a flame, because numerous species can be simultaneously detected at fixed nominal ion energy, it lacks the capacity of isomer separation. Also, fragmentation of labile species can be a problem. As a more advanced approach, PI-MBMS using VUV radiation from synchrotrons had been introduced into combustion experiments about a decade ago [29,46], its typical advantages including high energy resolution, isomer identification from photoionization efficiency (PIE) curves, and reduced fragmentation. Most recently, the arse-

nal of combustion diagnostics has been further expanded by the introduction of PEPICO spectroscopy to study combustion-related gas mixtures [47] and flames [48,49]. The approach has the potential to add another dimension of discrimination between different chemical species from detecting the electron–ion coincidences that occur upon individual ionization events.

PEPICO spectroscopy is a well-known technique [81-84] that has been widely applied for decades to state-selected core- and valence-shell excited/ionized molecules for the study of cation dissociation dynamics and for spectroscopic and thermochemical investigations. For the sake of directness, here we restrict the introduction of PEPICO to more recent literature on imaging techniques, and their combination to synchrotron tunable light sources, relevant to the following discussion [85-88]. In these experiments, photoionization (as for PI-MBMS) typically relies on brilliant, continuously tunable VUV light from synchrotrons in the 6 to 20 eV range where lie the ionization energies (and first excited electronic states) of the chemical products that one may want to probe. For a given mass, "T"PEPICO or "threshold" PEPICO spectra can be obtained with high signal intensity from scanning the photon energy over the ionization threshold, at fixed zero kinetic energy of the electrons. With velocity map imaging, zero kinetic energy electrons can be recorded as a focused spot on the detector, and electrons with velocities perpendicular to the extraction axis will appear as concentric rings around this central spot [83]. The imaging schemes are capable of multiplex electron energy and ion mass detection and have 100% transmission efficiency, so that electrons and ions can be detected with high signal intensities in a chemically relevant energy range. Recently, these techniques have been refined at different synchrotron facilities with the additional correlation of the ion position, which gives access to its translational energy [89,90].

Current PEPICO spectrometers at different synchrotrons combine high signal intensities with high electron and photon energy resolutions [50,85,86]. PEPICO spectroscopy is suited to detect reactive species including radicals, a capability that has been demonstrated e.g. in flash pyrolysis experiments [91-93].

For combustion studies, it is advantageous that the electron–cation pairs formed by photoionization carry specific information of the molecular structure from which they were derived. Species identification may either be obtained from photoelectron spectra (PES) upon scanning the photon energy or by recording velocity map images of the photoelectrons by keeping the photon energy fixed at a value above the ionization threshold of the species or group of species of interest. Mass-selected threshold photoelectron spectra (TPES), for the first time from a flame, for a number of combustion intermediates using an iPEPICO detection scheme have recently been reported by Oßwald et al. [48]. These spectra show distinct "fingerprint" information with respective vibrational progressions for each isomer, features which were demonstrated, for example, for the isomer pair of allene and propyne. To evaluate the potential of PEPICO spectroscopy in comparison with the more common PI-MBMS and EI-MBMS approaches, these techniques have recently been applied to study an ethene flame at comparable conditions using instruments at three different synchrotrons and a laboratory EI-MBMS setup [49].

Here, we report results with the PEPICO technique obtained in a fuel-rich DME-O_2-Ar flame at ϕ=1.6 and 33 mbar. The flame was chosen considering its generally clear and well-studied chemistry; furthermore, the conditions are almost identical to one of the flames of Wang et al. [35]. Again, we focus on formaldehyde, CH_2O, as the target species to illustrate the information available from such measurements. Figure 4 shows the electron velocity map image obtained in this flame at h=3.1 mm for m/z=30 corresponding to CH_2O; the signal was recorded at a fixed photon energy of 11.62 eV so that formaldehyde could be reliably ionized. In comparison to a scan across the ionization threshold, the PEPICO measurement at fixed photon energy is considerably less time-consuming. By applying suitable numerical procedures, the PES can be retrieved also from these fixed-energy data. The raw photoelectron signal is given in the left half of Fig. 4. Shown in the right half is the result after filtering of the image with the pBasex [94] algorithm, a procedure designed to perform an inverse Abel trans-

formation to reconstruct the original three-dimensional Newton sphere of expanding charged particles, provided that an axis of cylindrical symmetry is contained on the image plane. This procedure permits reconstruction of the angular distribution of the photoelectrons for a given mass, and yields in particular the photoelectron spectroscopy (PES). Concentric rings appear after inversion for the selected kinetic energy range of the photoelectrons, showing the respective vibrational progressions.

The mass-selected PES for formaldehyde at m/z=30, extracted by keeping only photoelectron–photoion coincidences for a single mass from the velocity map image recorded at a photon energy of 11.62 eV in Fig. 4, is given in Fig. 5. This complete PES was measured without the need for photon energy scanning. Note that, although we choose here to focus on m/z=30, the multiplexing capabilities of this technique allow for the simultaneous recording of the full PES of all the species ionized. The sharp peak identified in this spectrum with its maximum near 10.9 eV is in very good agreement with the ionization energy of 10.88 eV of formaldehyde [95]. Furthermore, the spectrum shows vibrational structure in good agreement with the PES spectrum in the 10.8-11.6 eV range reported by Baker et al. [96], which is given in Fig. 5 for comparison and from which an ionization energy of 10.88(4) eV was determined. In contrast to PIE spectra where ionization thresholds are indicated as steps or changes of slopes, photoelectron spectra show clear peaks for all transitions, demonstrating their discriminative power.

Because total ion yield at a given photon energy corresponds to the integral of the PES obtained at that same photon energy, the mass-resolved PES, measured at different heights above the burner, can be used to determine the relative mole fraction profile of a species. The formaldehyde profile in Fig. 6 was derived from a fixed-energy measurement of the PES at 10.98 eV and is compared to the result of Wang et al. [35], measured in a very similar DME flame with a stoichiometry of ϕ=1.63 at 33 mbar. The maximum mole fraction of CH_2O in this flame determined by EI-MBMS is ~0.02, with an experimental uncertainty of about 30%

[35]. The profiles in Fig. 6, scaled to the same maximum value, are in very good agreement in the region of the maximum and further downstream, with a sharper rise noted in the PEPICO experiment. Although measurement uncertainties for invasive experiments can include differences upon variations in sampling probe, burner, and burner housing geometries [97], the agreement seen here is encouraging.

PEPICO spectra determined at fixed photon energy such as reported here provide a multiplex advantage over the scanning mode using zero kinetic energy photons. With only few well-selected photon energies, identification and quantification for sets of relevant species may thus become routinely possible, provided their ionization thresholds, photoelectron spectra, and ionization cross sections are known. Compared to the convoluted appearance of PIE spectra for a given mass from PI-MBMS that will exhibit several steps if several species contribute to the signal, the sharp features in mass-selected PES offer superb discrimination useful for isomer separation, even if data are taken at fixed photon energy instead of using more time-consuming scans [49]. PEPICO spectroscopy, although experimentally involved, will thus offer advantages that are not available with current techniques for chemical combustion diagnostics [48,49].

3.3 Soot and soot precursor diagnostics in hydrocarbon flames using MS and HIM

Soot formation is one of the most intensely studied – and most complex – chemical reaction mechanisms in combustion [98-100]. Reliable prediction of soot formation with detailed combustion models that could link the flame precursor chemistry to the formed soot particle's structure and properties would greatly benefit the assessment of health risks and environmental influences. Currently, both ends of the particle formation process – the molecular reactions to form the first aromatic structures and the growth of particles once they are conceived – seem better understood than the regime between them [101,102], although efforts are made to link the gaseous molecular phase systematically with the nanoparticles resulting from the

growth process [103,104]. Several variants of mass spectrometry and particle characterization techniques have been used in attempts to diminish the gap between molecules and particles [45,105-108].

Here, we have investigated a non-premixed flame in an opposed-flow configuration to follow the buildup of small PAHs. Figure 7 shows a typical mass spectrum in the range of *m*/*z*=70-230, measured with probe-sampling MS in an atmospheric-pressure *n*-butane flame near the sooting region. The results may be compared to the analysis of an *i*-butene flame in the same configuration, described in [36]. It is evident from the insert in Fig. 7 that a large number of intermediates is formed, only a few of which are easily assigned. With the resolution of the mass spectrometer, potential oxygenated species cannot be distinguished by mass, and isomeric structures can only be determined in a number of cases with GC. The mass spectrum therefore serves as an illustration of the complexity of the chemical composition even in this rather limited mass range, which encompasses structures with up to four aromatic rings. One of the most prominent signals in the higher mass range in this spectrum is seen at *m*/*z*=202, which could include pyrene, one of the smallest PAH structures that can lead to dimerization. Already for the growth of benzene at *m*/*z*=78, several pathways are responsible, which have been discussed in the literature as starting points for further growth [100-102]. They include the so-called HACA (hydrogen abstraction acetylene addition) route as one of the most widely accepted mechanisms [109], which would manifest itself here by building blocks of *m*/*z*=24. Indeed, features at *m*/*z*=102 and at several corresponding higher masses are detected in the mass spectrum in Fig. 7.

As discussed also in [36], methyl can contribute to such growth processes, inferred from signals present in the spectrum at mass differences of *m*/*z*=14 from benzene (which would be consistent with loss of an H atom and CH_3 addition), e.g. at *m*/*z*=92 and 106. These signals include toluene (confirmed by GC) and potentially ethylbenzene as well as xylenes. Similarly, sequences that start from naphthalene (confirmed by GC) at *m*/*z*=128 could be interpreted in

terms of a methyl-involving growth pathway, with corresponding peaks at *m*/*z*=142 and 156 [36]. From the GC analysis, further identified compounds include styrene at *m/z*=104, indene at *m/z*=116, 1-methylnaphtalene and/or 2-methylnaphtalene at *m/z*=142, acenaphthylene at *m/z*=152, fluorene at *m/z*=166, and phenanthrene at *m/z*=178. No isomer identification was possible for the observed features at *m/z*=154 and 156. The latter could correspond to ethyl-substituted naphthalene, and biphenyl could contribute to the former. The rich mass spectrum with identification of condensed aromatic species, aromatic compounds with aliphatic side chains, and five- as well as six-membered rings, with saturated and unsaturated structures indicates that the pathways to higher-molecular growth are already manifold at the level of the molecular species and smaller aromatics identified here. Several drawbacks must be noted, however, with this analysis. On the one hand, the present sampling from the opposed-flow flame configuration does not permit the detection of radicals, and on the other, comparison with simulations would need more detailed assignments and, desirably, quantitative evaluation, which may demand theoretical support. Nevertheless, mass spectrometric analysis of non-premixed flames is well suited to further examine complex combustion situations.

While soot formation studies typically investigate the growth process along the sequence from the molecular precursors to the carbon structures, clusters, and nanoparticles, the opposite perspective is also attractive. From small soot particles, chemical compounds on their surface can be desorbed and analyzed [105-107] which will not only provide information on their reactivity and potential toxic properties but will also reveal features of the growth process that are compatible with such surface coverage. Bouvier et al. [105] have combined laser-induced incandescence (LII), laser-induced fluorescence (LIF), and laser desorption–laser ionization mass spectrometry (LD/LI/MS) to provide combined information on soot particles, PAHs in the gas phase, and molecular structures on the surfaces of the soot particles. Their LD/LI/MS spectra revealed a number of smaller PAHs in the range up to four rings, mostly belonging to the most stable thermodynamic structures or stabilomers [110]. Based upon a

number of calibrations and showing good agreement with the data from Apicella et al. [107], the combination of techniques has been applied to study soot formation in premixed methane flames [106]. Large PAH structures containing in the range of 60 carbon atoms have been identified, suggesting that not only homogeneous but also heterogeneous processes will play a role in the soot inception and growth sequences [106].

Clearly, there remains a need to characterize very small soot particle structures with sizes <10 nm, both regarding their morphological as well as their chemical properties. In our own work, we have recently used helium ion microscopy for the first time to characterize young soot [38,39]. This technique provides superior contrast and has enabled soft imaging of soot particle structures with features down to the 2 nm range without apparent changes after multiple exposures to the helium ion beam [38]. Figure 8 provides an overview of such morphological variations in soot particles collected at different heights in a premixed fuel-rich ϕ=2.07 ethene-oxygen-argon flame at atmospheric pressure that was characterized before by Abid et al. [37]. The image shows samples analyzed for heights of 0.5, 0.8, and 1.2 mm, reflecting further growth progressively with reaction time. At all heights, near-spherical particles were detected with sizes in the 4-7 nm range (surrounded by hexagons). Primary particles of 14-18 nm sizes (squares) occur at the same time as apparent aggregates (circles) with a more rugged structure. Size distributions evaluated from the HIM images were largely in favorable agreement with those determined by scanning mobility particle sizing (SMPS) in [37] for the same conditions. Geometric parameters of the detected particles were analyzed from a larger number of images that have provided information about the sphericity, circularity, and fractal dimension to illustrate particle properties in comparison with a perfect sphere. More detailed analyses with additional flame conditions were performed in a recent study [39], again using conditions that had been investigated by Abid et al. before [37]. All results indicate an important contribution of aggregation already in the very early stages of soot formation, demonstrated by significant deviations from spherical geometries. As a further result from these re-

cent investigations, no distinct variations of the geometric parameters were seen with increasing growth time or height, again underlining the coexistence of primary particles and aggregates throughout the growth process [38,39].

While such analyses accessible with advanced microscopy techniques that are new to combustion diagnostics may challenge some earlier assumptions regarding the growth process, chemical information is needed in addition. In recent investigations of soot formation, for very small nanoparticles of carbon to primary particles, different spectroscopic techniques were applied for a more in-depth characterization [101,111-113], including in particular X-ray photoelectron spectroscopy (XPS) and infrared spectroscopy. For soot from an ethene flame analogous to that of Abid et al. [37], Fig. 9 shows a number of vibrations identified from PM-IRRAS measurements; particles were collected at a height of 1.2 cm from the burner surface onto a gold-coated silicon wafer. The features were interpreted following the assignments by Cain et al. [113] and include prominently the aromatic CH stretch at 3045 cm^{-1}, several symmetric and asymmetric alkane stretch vibrations at 2960, 2928, and 2860 cm^{-1}, and the aromatic C=C vibration at 1595 cm^{-1}. Also, features involving oxygen are noted with the carbonyl (1718 cm^{-1}), C-O stretch (1068 cm^{-1}), and C-O-C (1288 cm^{-1}) vibrations. These correspond well with peaks of soot samples for the same flame conditions, analyzed with XPS [39]. It should be noted, however, that different sampling conditions were used for the XPS measurements, where thermophoretic sampling was applied similar to the sample collection for HIM, whereas for the PM-IRRAS measurements here, which need a larger particle density and different substrates, the probe technique described by Abid et al. [52] was used, with potentially different exposure to room air after sampling. The reactivity of the soot particles with respect to oxidation may furthermore depend on their size and growth history, and more detailed investigations are needed to understand such influences.

4. Summary and perspectives

The examples reported here have provided a short introduction into the application of several techniques that have only been recognized quite recently for combustion diagnostics. These studies have been devoted to contribute to investigations of pertinent chemical aspects of combustion processes under laboratory conditions, intended to assist in elucidating details of pollutant formation mechanisms. With two main examples, the detection of formaldehyde as a prominent air toxic, representative of carbonyl species that may be found in unregulated emissions, and the analysis of very small soot particles that are regarded as one of the most harmful classes of combustion emissions, it has been underlined that reliable quantitative measurements are seldom available from a single technique. Combinations of methods are essential to reveal details of the respective reaction processes.

In chemical combustion analysis, especially in systems with many intermediate species and structures, the investigations must often rely on qualitative information: even identification of species and comprehensive analysis of average features of particle ensembles may pose difficulties. Furthermore, it remains challenging to quantitatively measure one species in nominally "identical" conditions at several locations or with different techniques, and not all measurement strategies can be applied under the same flame conditions. Comparisons of results from non-invasive and probe-sampling techniques are often not satisfactory, and probe effects need to be assessed systematically. Whenever possible, it is preferable to rely on optical methods. Fortunately, the increasing availability of laser systems and techniques offer adequate choices.

In the attempt to provide high-quality data for model examination and development, researchers may thus profit not only from the established, working arsenal of combustion diagnostics, but also from the approaches described here and other newer instruments, measurement techniques, and procedures that conquer territories that were previously harder to access. With QCLAS, PEPICO, and HIM/PM-IRRAS, some examples were given how such tech-

niques can expand current combustion chemistry diagnostics. Much of the contributions to laboratory-based chemical insights must be tested under the practically relevant conditions. Such transfer to real-world combustion must often proceed via accurate modeling, where chemical complexity is still one of the largest obstacles, because computer simulations of highly involved geometries and time-changing flow fields cannot yet integrate the full chemical detail. Experimental advances in combustion diagnostics thus contribute another important perspective for the analysis of complex chemical systems in that they can determine the most crucial and sensitive aspects to be represented by reduced mechanisms for practical applications.

Acknowledgements

The authors would like to acknowledge contributions of several team members in the research described here. We are especially grateful to Lena Ruwe for her assistance with soot sampling and some related diagnostics, as well as to Alexander Lackner with his help in QCLAS experiments. Furthermore, we thank Dr. Gustavo Garcia and Dr. Laurent Nahon, SOLEIL, for the opportunity to couple a flame experiment to the PEPICO spectrometer at SOLEIL and for their invaluable assistance in the introduction to the instrument and data analysis. Also, we acknowledge access to the IRRAS instrumentation in the laboratory of Prof. Armin Gölzhäuser. Inspiring discussions with Prof. Hai Wang, Stanford University, USA, Dr. André Beyer, and Dr. Kai Moshammer are gratefully acknowledged. NH is supported by the Division of Chemical Sciences, Geosciences, and Biosciences, the Office of Basic Energy Sciences, United States Department of Energy, and acknowledges the Alexander von Humboldt Stiftung for partial support of his stay in Bielefeld. Sandia is a multiprogram laboratory operated by Sandia Corporation, a Lockheed Martin Company, for the National Nuclear Security Administration, under contract DE-AC04-94AL85000.

References

[1] O. Boucher, O.D. Randall, P. Artaxo, C. Bretherton, G. Feingold, P. Forster, V.-M. Kerminen, Y. Kondo, H. Liao, U. Lohmann, P. Rasch, S.K. Satheesh, S. Sherwood, B. Stevens, X.Y. Zhang, 2013: Clouds and Aerosols. In: *Climate Change 2013: The Physical Science Basis. Contribution of Working Group I to the Fifth Assessment Report of the Intergovernmental Panel on Climate Change* [Stocker, T.F., D. Qin, G.-K. Plattner, M. Tignor, S.K. Allen, J. Boschung, A. Nauels, Y. Xia, V. Bex and P.M. Midgley (eds.)]. Cambridge University Press, Cambridge, United Kingdom and New York, NY, USA.

[2] N.A.H. Janssen, M.E. Gerlofs-Nijland, T. Lanki, R.O. Salonen, F. Cassee, G. Hoek, P. Fischer, B. Brunekreef, M. Krzyzanowski, *Health effects of black carbon*, World Health Organization 2012, http://www.euro.who.int/__data/assets/pdf_file/0004/162535/e96541.pdf

[3] L.G. Anderson, Energy Environ. Sci. 2 (2009) 1015-1037.

[4] S.M. Corrêa, G. Arbilla, E.M. Martins, S.L. Quitério, C. de Souza Guimarães, L.V. Gatti, Atmos. Environ. 44 (2010) 2302–2308.

[5] O. Deutschmann, J.-D. Grunwaldt, Chem. Ing. Tech. 85 (2013) 595–617.

[6] S.C. Davis, S.W. Diegel, R.G. Boundy, *Transportation Energy Data Book Edition 31*, Oak Ridge National Laboratory, July 2012, http://cta.ornl.gov/data .

[7] H. Cai, S. D. Xie, Atmos. Chem. Phys. 9 (2009) 6983–7002.

[8] US Energy Information Administration, *International Energy Outlook 2011*, http://www.eia.gov/emeu/international .

[9] *BP Statistical Review of World Energy June 2013,* http://www.bp.com/content/dam/bp/pdf/statistical-review/statistical_review_of_world_energy_2013.pdf .

[10] T. Li, H. Ogawa, J. Autom. Engr. 223 (2009) 673–683.

[11] B.-Q. He, M.-B. Liu, J. Yuan, H. Zhao, Fuel 108 (2013) 668–674.

[12] B.-Q. He, J. Yuan, M.-B. Liu, H. Zhao, Fuel 115 (2014) 758–764.

[13] C.K. Westbrook, Y. Mizobuchi, T.J. Poinsot, P.J. Smith, J. Warnatz, Proc. Combust. Inst. 30 (2005) 125–157.

[14] P.A. Vlasov, J. Warnatz, Proc. Combust. Inst. 29 (2002) 2335–2341.

[15] G.L. Agafonov, I. Naydenova, P.A. Vlasov, J. Warnatz, Proc. Combust. Inst. 31 (2007) 575–583.

[16] J. Warnatz, U. Maas, R.W. Dibble, *Combustion*, 4th ed., Springer, Berlin, Heidelberg, New York, 2006.

[17] T. Lu, C.K. Law, Prog. Energy Combust. Sci. 35 (2009) 192–215.

[18] A.C. Eckbreth, *Laser Diagnostics for Combustion Temperature and Species*, 2nd ed., Gordon and Breach, Amsterdam, 1996.

[19] K. Kohse-Höinghaus, J.B. Jeffries, eds., *Applied Combustion Diagnostics*, Taylor & Francis, New York, London, 2002.

[20] M.A. Linne, *Spectroscopic Measurements*, Academic Press, London, 2002.

[21] K. Kohse-Höinghaus, R.S. Barlow, M. Aldén, J. Wolfrum, Proc. Combust. Inst. 30 (2005) 89–123.

[22] R.K. Hanson, Proc. Combust. Inst. 33 (2011) 1–40.

[23] N. Hansen, T.A. Cool, P.R. Westmoreland, K. Kohse-Höinghaus, Prog. Energy Combust. Sci. 35 (2009) 168–191.
[24] C.A. Taatjes, N. Hansen, D.L. Osborn, K. Kohse-Höinghaus, T.A. Cool, P.R. Westmoreland, Phys. Chem. Chem. Phys. 10 (2008) 20–34.
[25] Y. Li, F. Qi, Acc. Chem. Res. 43 (2010) 68–78.
[26] S.H. Dürrstein, M. Aghsaee, L. Jerig, M. Fikri, C. Schulz, Rev. Sci. Instrum. 82 (2001) 084103.
[27] H. Guo, W. Sun, F.M. Haas, T. Farouk, F.L. Dryer, Y. Ju, Proc. Combust. Inst. 34 (2013) 573–581.
[28] F. Battin-Leclerc, O. Herbinet, P.-A. Glaude, R. Fournet, Z. Zhou, L. Deng, H. Guo, M. Xie, F. Qi, Proc. Combust. Inst. 34 (2013) 325–331.
[29] C.A. Taatjes, N. Hansen, A. McIlroy, J.A. Miller, J.P. Senosiain, S.J. Klippenstein, F. Qi, L. Sheng, Y. Zhang, T.A. Cool, J. Wang, P.R. Westmoreland, M.E. Law, T. Kasper, K. Kohse-Höinghaus, Science 308 (2005) 1887–1889.
[30] F. Qi, Proc. Combust. Inst. 34 (2013) 33–63.
[31] B. Yang, P. Oßwald, Y. Li, J. Wang, L. Wei, Z. Tian, F. Qi, K. Kohse-Höinghaus, Combust. Flame 148 (2007) 198–209.
[32] N. Hansen, T. Kasper, S.J. Klippenstein, P.R. Westmoreland, M.E. Law, C.A. Taatjes, K. Kohse-Höinghaus, J. Wang, T.A. Cool, J. Phys. Chem. A 111 (2007) 4081–4092.
[33] Patrick Nau, Entwicklung und Optimierung absorptionsspektroskopischer Techniken zur Untersuchung von Verbrennungsprozessen, PhD Thesis (in German), Bielefeld University, October 2012; Shaker-Verlag, Aachen, 2012.
[34] Julia Koppmann, Tomographische Absorptionsuntersuchungen im mittleren Infrarotbereich mittels Quantenkaskadenlasern zur Spezies- und Temperaturbestimmung in Flammen, M. Sc. Thesis (in German), Bielefeld University, November 2012.
[35] J. Wang, M. Chaos, B. Yang, T.A. Cool, F.L. Dryer, T. Kasper, N. Hansen, P. Oßwald, K. Kohse-Höinghaus, P.R. Westmoreland, Phys. Chem. Chem. Phys. 11 (2009) 1328–1339.
[36] M. Schenk, N. Hansen, H. Vieker, A. Beyer, A. Gölzhäuser, K. Kohse-Höinghaus, accepted for presentation at the 35th International Symposium on Combustion, San Francisco, USA, August 3-8, 2014, and Proc. Combust. Inst. 35 (2014), submitted for publication.
[37] A.D. Abid, N. Heinz, E.D. Tolmachoff, D.J. Phares, C.S. Campbell, H. Wang, Combust. Flame 154 (2008) 775–788.
[38] M. Schenk, S. Lieb, H. Vieker, A. Beyer, A. Gölzhäuser, H. Wang, K. Kohse-Höinghaus, ChemPhysChem 14 (2013) 3248–3254.
[39] M. Schenk, S. Lieb, H. Vieker, A. Beyer, A. Gölzhäuser, H. Wang, K. Kohse-Höinghaus, accepted for presentation at the 35th International Symposium on Combustion, San Francisco, USA, August 3-8, 2014, and Proc. Combust. Inst. 35 (2014), submitted for publication.
[40] C.J. Dasch, Appl. Opt. 31 (1992) 1146–1152.
[41] R. Villarreal, P.L. Varghese, Appl. Opt. 44 (2005) 6786–6795.
[42] M. Schenk, L. Leon, K. Moshammer, P. Oßwald, T. Zeuch, L. Seidel, F. Mauss, K. Kohse-Höinghaus, Combust. Flame 160 (2013) 487–503.

[43] P. Oßwald, K. Kohse-Höinghaus, U. Struckmeier, T. Zeuch, L. Seidel, L. Leon, F. Mauss, Z. Phys. Chem. 225 (2011) 1029–1054.
[44] A. Brockhinke, A. Bülter, J.C. Rolon, K. Kohse-Höinghaus, Appl. Phys. B 72 (2001) 491–496.
[45] S.A. Skeen, H.A. Michelsen, K.R. Wilson, D.M. Popolan, A. Violi, N. Hansen, J. Aerosol Sci. 58 (2013) 86–102.
[46] T.A. Cool, A. McIlroy, F. Qi, P.R. Westmoreland, L. Poisson, D.S. Peterka, M. Ahmed, Rev. Sci. Instrum. 76 (2005) 094102.
[47] A. Bodi, P. Hemberger, D.L. Osborn, B. Sztaray, J. Phys. Chem. Lett. 4 (2013) 2948–2952.
[48] P. Oßwald, P. Hemberger, T. Bierkandt, E. Akyildiz, M. Köhler, A. Bodi, T. Kasper, Rev. Sci. Instrum. 85 (2013) 025101.
[49] D. Felsmann, K. Moshammer, J. Krüger, A. Lackner, A. Brockhinke, T. Kasper, T. Bierkandt, E. Akyildiz, N. Hansen, A. Lucassen, P. Oßwald, M. Köhler, G.A. Garcia, L. Nahon, P. Hemberger, A. Bodi, T. Gerber, K. Kohse-Höinghaus, accepted for presentation at the 35th International Symposium on Combustion, San Francisco, USA, August 3-8, 2014, and Proc. Combust. Inst. 35 (2014), submitted for publication.
[50] G.A. Garcia, B.K. Cunha de Miranda, M. Tia, S. Daly, L. Nahon, Rev. Sci. Instrum. 84 (2013) 053112.
[51] C.A. Schneider, W.S. Rasband, K.W. Eliceiri, Nat. Methods 9 (2012) 671–675.
[52] A.D. Abid, J. Camacho, D.A. Sheen, H. Wang, Combust. Flame 156 (2009) 1862–1870.
[53] C. Arcoumanis, C. Bae, R. Crookes, E. Kinoshita, Fuel 87 (2008) 1014–1030.
[54] C. Togbé, L.-S. Tran, D. Liu, D. Felsmann, P. Oßwald, P.-A. Glaude, B. Sirjean, R. Fournet, F. Battin-Leclerc, K. Kohse-Höinghaus, Combust. Flame 161 (2014) 780–797.
[55] Z. Zhu, D.K. Li, J. Liu, Y.J. Wei, S.H. Liu, Appl. Therm. Engr. 35 (2012) 9–14.
[56] H.J. Curran, W.J. Pitz, C.K. Westbrook, P. Dagaut, J.-C. Boettner, M. Cathonnet, Int. J. Chem. Kinet. 30 (1998) 229–241.
[57] X.L. Zheng, T.F. Lu, C.K. Law, C.K. Westbrook, H.J. Curran, Proc. Combust. Inst. 30 (2005) 1101–1109.
[58] T. Wada, A. Sudholt, H. Pitsch, N. Peters, Combust. Theory Model. 17 (2013) 906–934.
[59] H. Guo, W. Sun, F.M. Haas, T. Farouk, F.L. Dryer, Y. Ju, Proc. Combust. Inst. 34 (2013) 573–581.
[60] K. Zhang, K. Moshammer, P. Oßwald, K. Kohse-Höinghaus, Proc. Combust. Inst. 34 (2013) 763–770.
[61] F. Herrmann, B. Jochim, P. Oßwald, L. Cai, H. Pitsch, K. Kohse-Höinghaus, Combust. Flame 161 (2014) 384–397.
[62] S.L. Fischer, F.L. Dryer, H.J. Curran, Int. J. Chem. Kinet. 32 (2000) 713–740.
[63] H.J. Curran, S.L. Fischer, F.L. Dryer, Int. J. Chem. Kinet. 32 (2000) 741–759.
[64] Z. Zhao, M. Chaos, F.L. Dryer, Int. J. Chem. Kinet. 40 (2008) 1–18.
[65] W.K. Metcalfe, S. Burke, S. Ahmed, H.J. Curran, Int. J. Chem. Kinet. 45 (2013) 638–675.

[66] D. Liu, J. Santner, C. Togbé, D. Felsmann, J. Koppmann, A. Lackner, X. Yang, X. Shen, Y. Ju, K. Kohse-Höinghaus, Combust. Flame 160 (2013) 2654–2668.
[67] F. Herrmann, P. Oßwald, K. Kohse-Höinghaus, Proc. Combust. Inst. 34 (2013) 771–778.
[68] B. Brumfield, W. Sun, Y. Ju, G. Wysocki, J. Phys. Chem. Lett. 4 (2013) 872–876.
[69] P.A. Skovorodko, A.G. Tereshchenko, O.P. Korobeinichev, D.A. Knyazkov, A.G. Shmakov, Combust. Theory Model. 17 (2013) 1–24.
[70] U. Struckmeier, P. Oßwald, T. Kasper, L. Böhling, M. Heusing, M. Köhler, A. Brockhinke, K. Kohse-Höinghaus, Z. Phys. Chem. 223 (2009) 503–537.
[71] V. Gururajan, K. Kohse-Höinghaus, F. Egolfopoulos, accepted for presentation at the 35th International Symposium on Combustion, San Francisco, USA, August 3-8, 2014, and Proc. Combust. Inst. 35 (2014), submitted for publication.
[72] W. Ren, A. Farooq, D. Davidson, R.K. Hanson, Appl. Phys. B 107 (2012) 849–860.
[73] R.M. Spearrin, C.S. Goldenstein, J.B. Jeffries, R.K. Hanson, Appl. Opt. 53 (2014) 1938–1946.
[74] M.B. Sajid, E. Es-Sebbar, T. Javed, C. Fittschen, A. Farooq, Int. J. Chem. Kinet. 46 (2014) 275–284.
[75] J. Koppmann, A. Lackner, P. Nau, A. Brockhinke, K. Kohse-Höinghaus, 8th U.S. National Combustion Meeting, Park City, Utah, May 19-22, 2013.
[76] P. Nau, J. Koppmann, A. Lackner, A. Brockhinke, Appl. Phys. B (2014), submitted for publication.
[77] D. Liu, C. Togbé, L.-S. Tran, D. Felsmann, P. Oßwald, P. Nau, J. Koppmann, A. Lackner, P.-A. Glaude, B. Sirjean, R. Fournet, F. Battin-Leclerc, K. Kohse-Höinghaus, Combust. Flame 161 (2014), 748–765.
[78] P. Nau, J. Koppmann, A. Lackner, A. Brockhinke, K. Kohse-Höinghaus, Appl. Phys. B (2014) submitted for publication.
[79] D. G. Goodwin, CANTERA C++ User's Guide, 2002, Chem.Vap. Depos. XVI and EuroCVD 14 (2003) 08.
[80] HITRAN, http://www.cfa.harvard.edu/hitran/, 2008 and HITEMP, http://www.cfa.harvard.edu/hitemp/, 2010.
[81] C.J. Danby, J.H.D. Eland, Int. J. Mass Spectrom Ion Phys. 8 (1972) 153–161.
[82] B. Brehm, J.H.D. Eland, R. Frey, A. Küstler, Int. J. Mass Spectrom Ion Phys. 12 (1973) 213–224.
[83] T. Baer, Y. Li, Int. J. Mass Spectrom. 219 (2002) 381–389.
[84] B. Sztáray, T. Baer, Rev. Sci. Instrum. 74 (2003) 3763–3768.
[85] G.A. Garcia, H. Soldi-Lose, L. Nahon, Rev. Sci. Instrum. 80 (2009) 023102.
[86] A. Bodi, M. Johnson, T. Gerber, Z. Gengeliczki, B. Sztáray, T. Baer, Rev. Sci. Instrum. 80 (2009) 034101.
[87] X. Tang, X. Zhou, M. Niu, S. Liu, J. Sun, X. Shan, F. Liu, L. Sheng, Rev. Sci. Instrum. 80 (2009) 113101.
[88] P. O'Keeffe, P. Bolognesi, M. Coreno, A. Moise, R. Richter, G. Cautero, L. Stebel, R. Sergo, L. Pravica, Y. Ovcharenko, L. Avaldi, Rev. Sci. Instrum. 82 (2011) 033109.
[89] A. Bodi, P. Hemberger, T. Gerber, B. Sztáray, Rev. Sci. Instrum. 83 (2012) 083105.
[90] G.A. Garcia, B.K. Cunha de Miranda, M. Tia, S. Daly, L. Nahon, Rev. Sci. Instrum. 84 (2013) 053112.

[91] M. Steinbauer, P. Hemberger, I. Fischer, A. Bodi, ChemPhysChem 12 (2011) 1795–1797.
[92] P. Hemberger, M. Steinbauer, M. Schneider, I. Fischer, M. Johnson, A. Bodi, T. Gerber, J. Phys. Chem. A 114 (2010) 4698–4703.
[93] P. Hemberger, M. Lang, B. Noller, I. Fischer, C. Alcaraz, B.K. Cunha de Miranda, G.A. Garcia, H. Soldi-Lose, J. Phys. Chem. A 115 (2011) 2225–2230.
[94] G.A. Garcia, L. Nahon, I. Powis, Rev. Sci. Instrum. 75 (2004) 4989–4996.
[95] NIST Webbook Chemistry, *Ionization energetics data*, compiled by S.G. Lias, H.M. Rosenstock, K. Draxl, B.W. Steiner, J.T. Herron, J.L. Holmes, R.D. Levin, J.F. Liebman, S.A. Kafafi, http://webbook.nist.gov/chemistry/
[96] A.D. Baker, C. Baker, C.R. Brundle, D.W. Turner, Int. J. Mass Spectrom. Ion Phys. 1 (1968) 285–301.
[97] F. Egolfopoulos, N. Hansen, Y. Ju, K. Kohse-Höinghaus, C.K. Law, F. Qi, Prog. Energy Combust. Sci. 2014, doi:10.1016/j.pecs.2014.04.004.
[98] B.S. Haynes, H. Gg. Wagner, Prog. Energy Combust. Sci. 7 (1981) 229–273.
[99] A. D'Anna, Proc. Combust. Inst. 32 (2009) 593–613.
[100] H. Wang, Proc. Combust. Inst. 33 (2011) 41–67.
[101] H. Bockhorn, A. D'Anna, A.F. Sarofim, H. Wang (Eds.), *Combustion Generated Fine Carbonaceous Particles*, KIT Scientific Publishing, 2009.
[102] C.S. McEnally, L.D. Pfefferle, B. Atakan, K. Kohse-Höinghaus, Prog. Energy Combust. Sci. 32 (2006) 247–294.
[103] S.-H. Chung, A. Violi, Proc. Combust. Inst. 33 (2011) 693–700.
[104] D. Chen, Z. Zainuddin, E. Yapp, J. Ackroyd, S. Mosbach, M. Kraft, Proc. Combust. Inst. 32 (2013) 1827–1835.
[105] Y. Bouvier, C. Mihesan, M. Ziskind, E. Therssen, C. Focsa, J.F. Pauwels, P. Desgroux, Proc. Combust. Inst. 31 (2007) 841–849.
[106] A. Faccinetto, P. Desgroux, M. Ziskind, E. Therssen, C. Focsa, Combust. Flame 158 (2011) 227–239.
[107] B. Apicella, A. Carpentieri, M. Alfè, R. Barbella, A. Tregrossi, P. Pucci, A. Ciajolo, Proc. Combust. Inst. 31 (2007) 547–553.
[108] S.A. Skeen, B. Yang, H.A. Michelsen, J.A. Miller, A. Violi, N. Hansen, Proc. Combust. Inst. 34 (2013) 1067–1075.
[109] J. Appel, H. Bockhorn, M. Frenklach, Combust. Flame 121 (2000) 122–136.
[110] S. Stein, A. Farr, J. Phys. Chem. 89 (1985) 3714–3725.
[111] C.K. Gaddam, R.L. Vander Wal, Combust. Flame 160 (2013) 2517–2528.
[112] M. Alfè, B. Apicella, R. Barbella, J.-N. Rouzaud, A. Tregrossi, A. Ciajolo, Proc. Combust. Inst. 32 (2009) 697–704.
[113] J.P. Cain, P.L. Gassman, H. Wang, A. Laskin, Phys. Chem. Chem. Phys. 12 (2010) 5206–5218.

Figure captions

Figure 1: Temperature, CO and CO_2 mole fractions as a function of height above burner measured by QCLAS in DME-O_2-Ar flames of two different stoichiometries, using the conditions of Wang et al. [35]; results from [35] obtained with EI-MBMS and simulations using the model by Zhao et al. [64] are included for comparison.

Figure 2: Spectrum of CH_2O from QCLAS experiment taken at h=0.7 mm in the rich DME-O_2-Ar flame and simulation using the HITRAN/HITEMP databases [80].

Figure 3: CH_2O mole fraction profiles in the two DME-O_2-Ar flames. QCLAS results are compared with those obtained by Wang et al. [35] and with predictions by the model of Zhao et al. [64], using unperturbed temperature profiles as input file.

Figure 4: Velocity map image recorded at a fixed photon energy of 11.62 eV and filtered for mass 30, corresponding to CH_2O, obtained in a ϕ=1.6 DME-O_2-Ar flame at h=3.1 mm. *Left*: raw data, *right:* after treatment by the pBasex [94] inversion algorithm.

Figure 5: Photoelectron spectrum of CH_2O in a ϕ=1.6 DME flame at h=3.1 mm in comparison with a reference spectrum by Baker et al. [96]. The spectrum has been obtained by processing the velocity map image in Fig. 4 and has a resolution of 0.08 eV.

Figure 6: Height-resolved integrated CH_2O photoelectron signal at m/z=30, obtained at fixed photon energy of 10.98 eV in a ϕ=1.6 DME-O_2 flame (25% Ar) at 33 mbar, compared with CH_2O mole fraction from EI-MBMS in a ϕ=1.63 DME-O_2 flame (25.5% Ar) at 33 mbar from [35]. Two independent experimental setups were used with identical burner dimensions but slightly different sampling geometries.

Figure 7: Mass spectrum from a non-premixed *n*-butane flame near the sooting region.

Figure 8: Morphological variations of nascent soot which was collected at heights of 0.5, 0.8, and 1.2 cm and imaged by HIM, showing representative primary and aggregate structures. Particles shown in the hexagons are in the apparent size range of 4-8 nm, and those in

the squares are 14-18 nm. Particles shown in the circles are apparent aggregates. From [38] with permission.

Figure 9: PM-IRRAS spectrum of nascent soot on a gold-coated silicon wafer; soot was collected from a C_2H_4 flame at the condition C3 of [37] at 1.2 cm from the burner surface; peak identification was performed according to [113].

Figure 1: Temperature, CO and CO_2 mole fractions as a function of height above burner measured by QCLAS in DME-O_2-Ar flames of two different stoichiometries, using the conditions of Wang et al. [35]; results from [35] obtained with EI-MBMS and simulations using the model by Zhao et al. [64] are included for comparison.

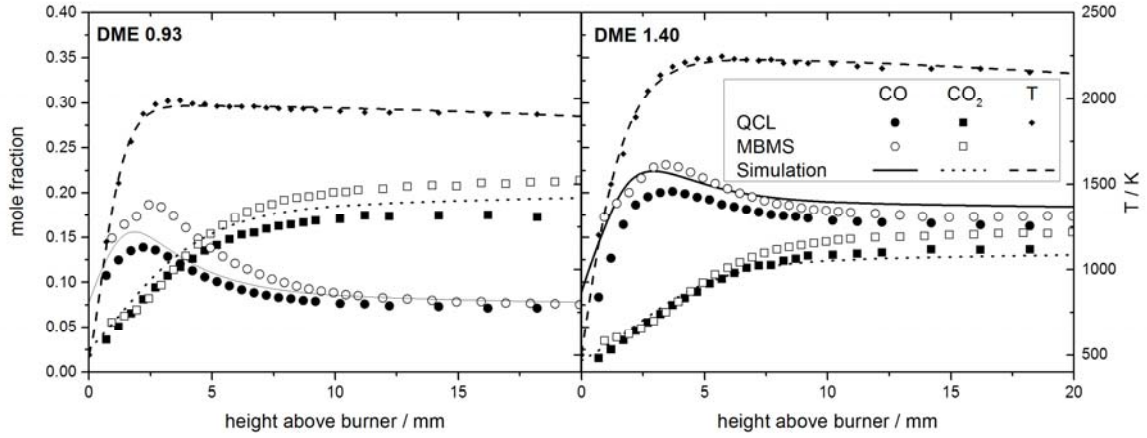

Figure 2: Spectrum of CH_2O from QCLAS experiment taken at *h*=0.7 mm in the rich DME-O_2-Ar flame and simulation using the HITRAN/HITEMP databases [80].

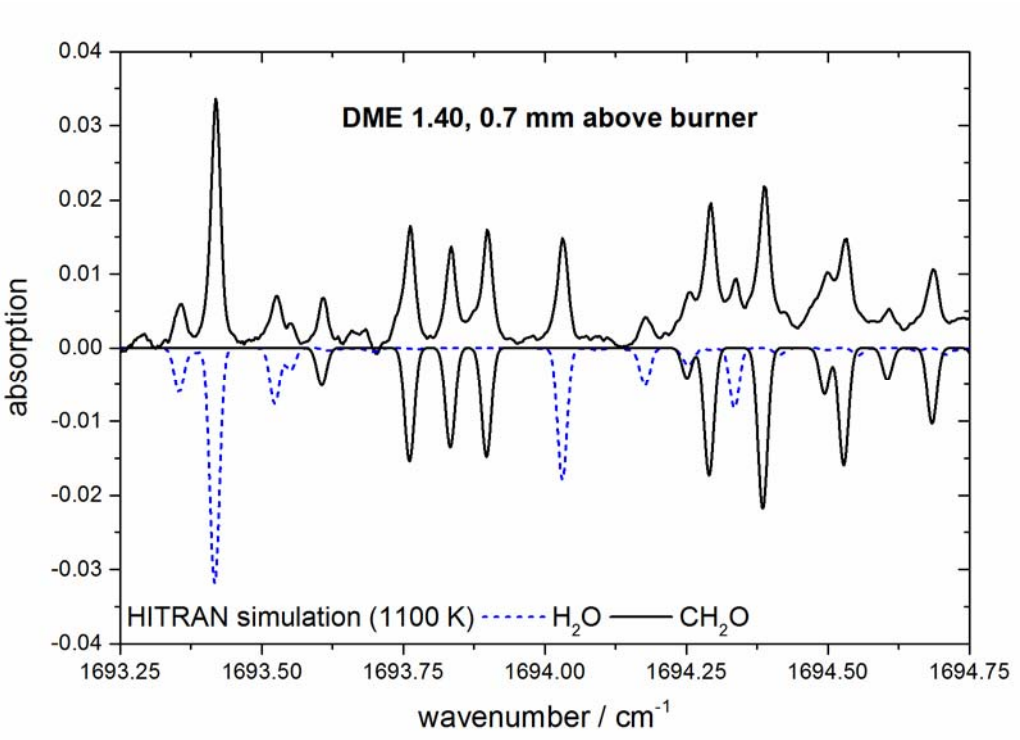

Figure 3: CH_2O mole fraction profiles in the two DME-O_2-Ar flames. QCLAS results are compared with those obtained by Wang et al. [35] and with predictions by the model of Zhao et al. [64], using unperturbed temperature profiles as input file.

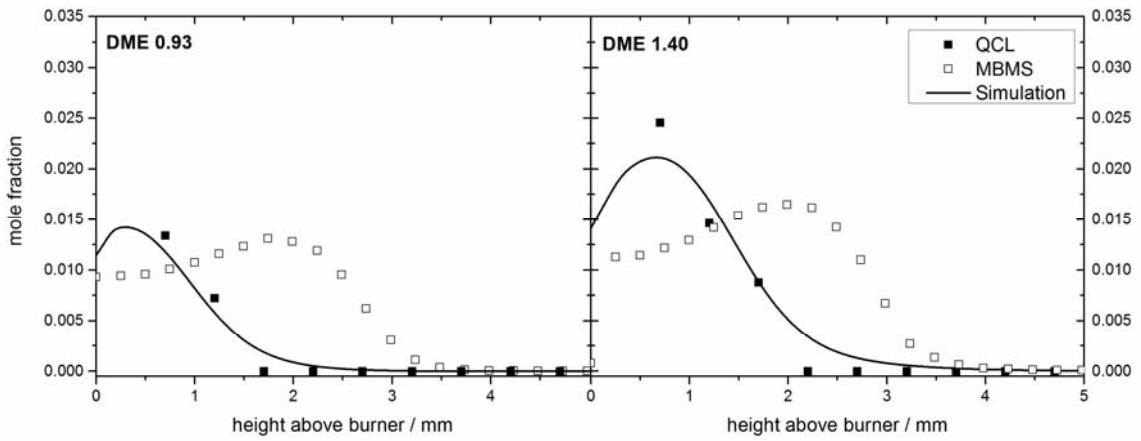

Figure 4: Velocity map image recorded at a fixed photon energy of 11.62 eV and filtered for mass 30, corresponding to CH_2O, obtained in a ϕ=1.6 DME-O_2-Ar flame at *h*=3.1 mm. *Left*: raw data, *right:* after treatment by the pBasex [94] inversion algorithm.

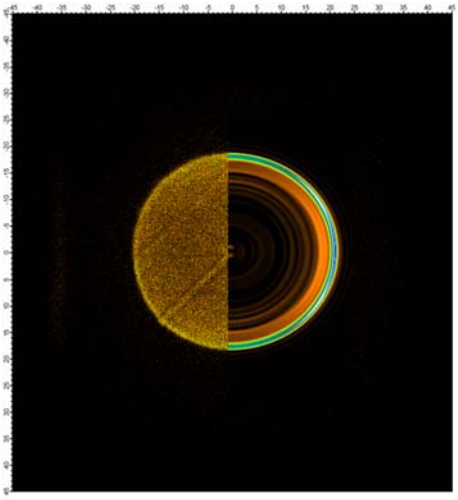

Figure 5: Photoelectron spectrum of CH_2O in a ϕ=1.6 DME flame at *h*=3.1 mm in comparison with a reference spectrum by Baker et al. [96]. The spectrum has been obtained by processing the velocity map image in Fig. 4 and has a resolution of 0.08 eV.

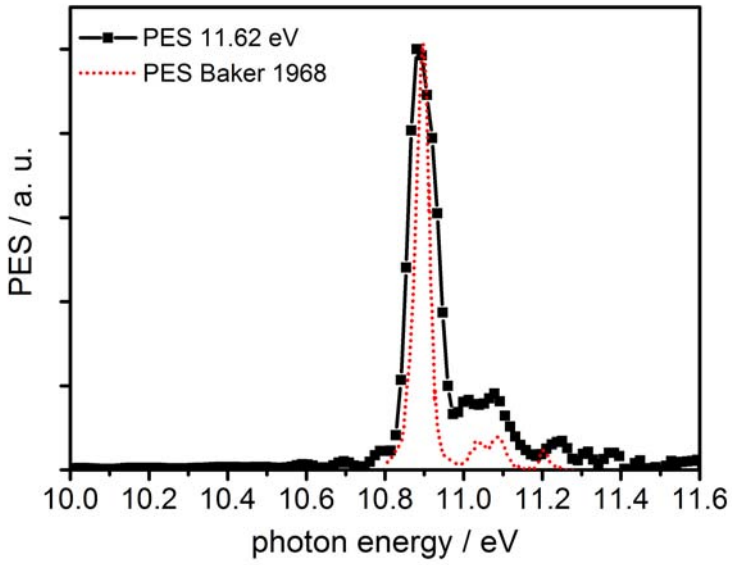

Figure 6: Height-resolved integrated CH_2O photoelectron signal at m/z=30, obtained at fixed photon energy of 10.98 eV in a ϕ=1.6 DME-O_2 flame (25% Ar) at 33 mbar, compared with CH_2O mole fraction from EI-MBMS in a ϕ=1.63 DME-O_2 flame (25.5% Ar) at 33 mbar from [35]. Two independent experimental setups were used with identical burner dimensions but slightly different sampling geometries.

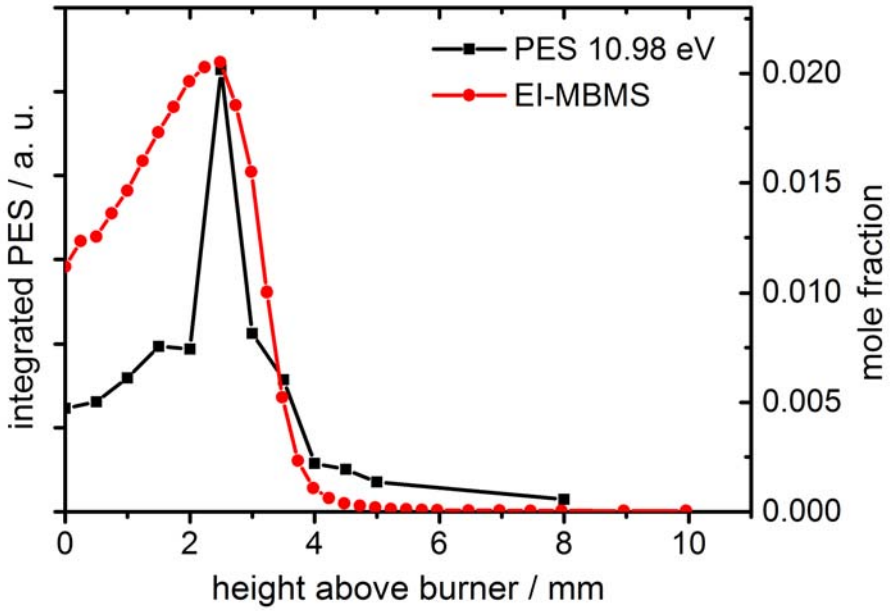

Figure 7: Mass spectrum from a non-premixed *n*-butane flame near the sooting region.

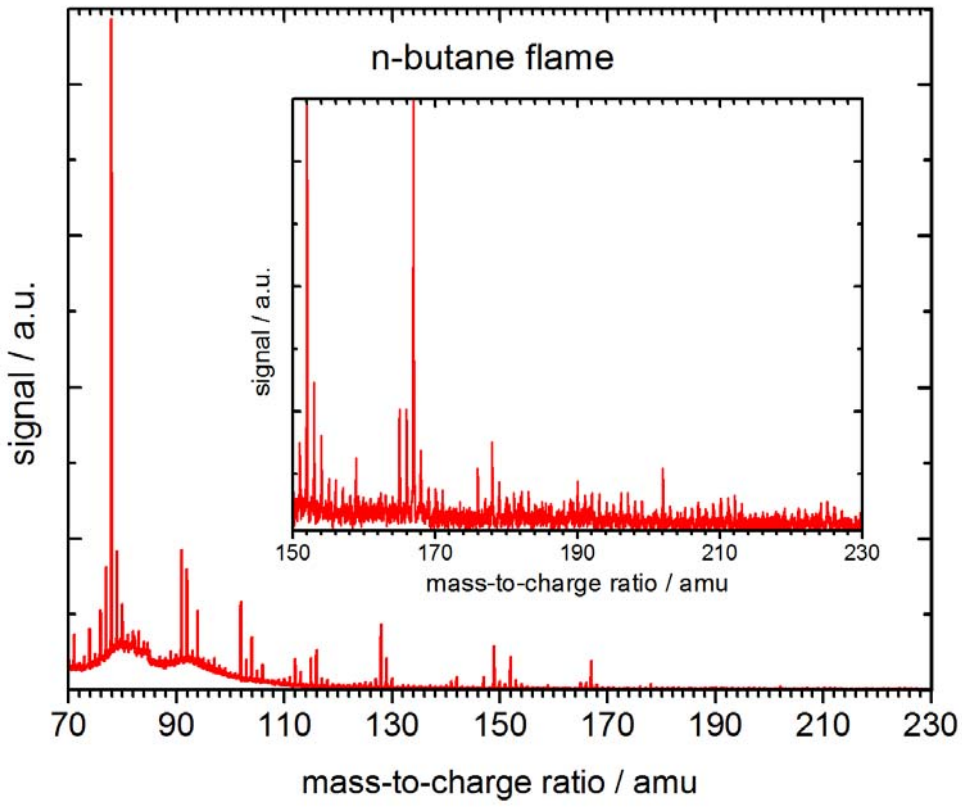

Figure 8: Morphological variations of nascent soot which was collected at heights of 0.5, 0.8, and 1.2 cm and imaged by HIM, showing representative primary and aggregate structures. Particles shown in the hexagons are in the apparent size range of 4-8 nm, and those in the squares are 14-18 nm. Particles shown in the circles are apparent aggregates. From [38] with permission.

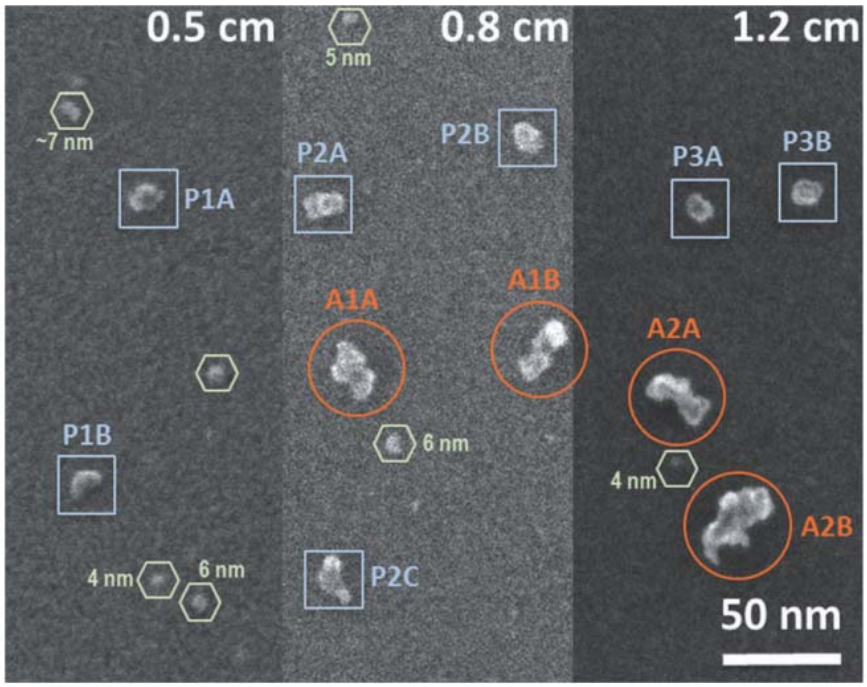
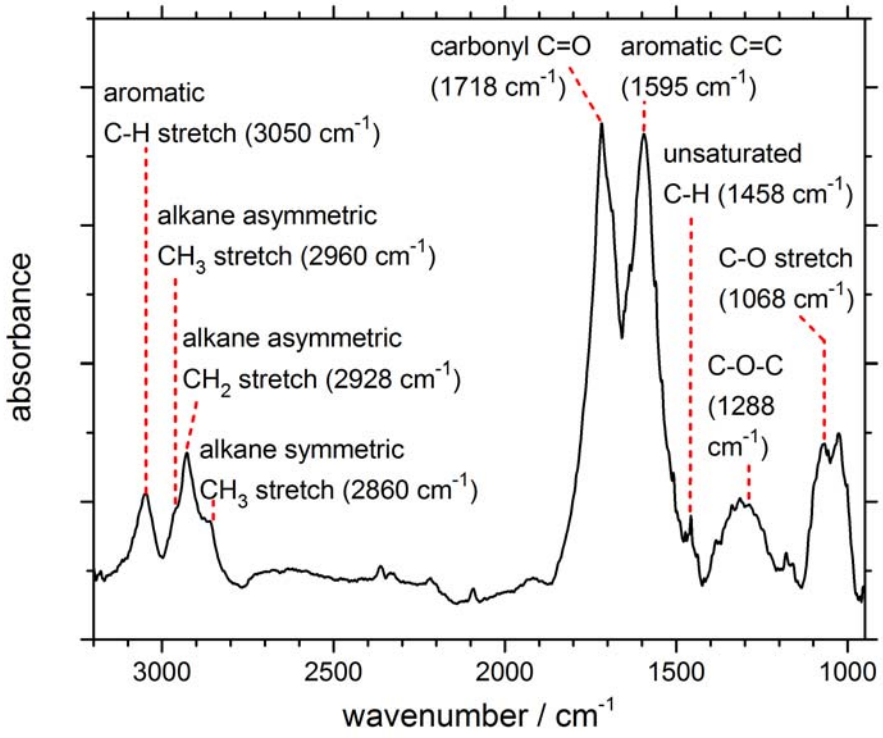
Figure 9: PM-IRRAS spectrum of nascent soot on a gold-coated silicon wafer; soot was collected from a C_2H_4 flame at the condition C3 of [37] at 1.2 cm from the burner surface; peak identification was performed according to [113].